Progress In Electromagnetics Research M, Vol. 41, 177–188, 2015

Modeling and Analysis of Halbach Magnetized Permanent-Magnets Machine by Using Lumped Parameter Magnetic Circuit Method

Guohai Liu, Mingming Shao, Wenxiang Zhao*, Jinghua Ji, Qian Chen, and Qian Feng

Abstract—Permanent-magnets (PMs) with tangential and parallel magnetization directions are combined in the Halbach PM (HPM) machine, which can offer high performances. However, the existing lumped parameter magnetic circuit (LPMC) model can only calculate one PM magnetization direction, namely either tangential direction or parallel direction. The key of this paper is to propose a method to divide and establish equivalent magnetic motive force (MMF) for HPM machine with both tangential and parallel magnetizations. Then, a LPMC model, using equivalent MMF, is developed to predict the electromagnetic performances for a four-phase HPM machine. In order to verify the effectiveness of the proposed LPMC model, a 6-pole/8-slot 15 kW HPM prototype is built. The comparative results of the proposed LPMC model, two-dimensional (2D) FEM and the experiments verify the effectiveness of the proposed LPMC model.

1. INTRODUCTION

Halbach permanent-magnet (HPM) can inherently offer sinusoidal air gap field, negligible cogging torque, sinusoidal air-gap field distribution, back-electromotive force (back-EMF) and needless of rotor back-iron, due to self-shielding magnetization [1]. Hence, these HPM machines have been extensively applied in many electric drive fields.

The lumped parameter magnetic circuit (LPMC) models have been used to predict the electromagnetic performances in many PM machines, except HPM machine, at the design stage because of its many merits [2–22]. A LPMC model of a switched reluctance machine was presented in [2–7]. This LPMC model construction is simple because there is no PM in switched reluctance machine. In [8–15], the LPMC models for doubly salient PM, axial-flux PM, spoke-type PM and flux-switching PM machines were built. The magnetization directions of their PMs are tangential. Approximatively, these PMs can be considered as rectangle sources. Also, the surface-mounted PM (SPM) and the interior PM machines were analyzed by using LPMC method in [16–22]. The magnetization direction of their PMs is radial or parallel. In summary, the above-mentioned LPMC models have only one PM magnetization (tangential or parallel). Since their PMs are separated, the magnetic motive force (MMF) of PMs can be considered as a constant. However, for the HPM machine, both tangential and parallel magnetizations are adopted, and the MMF of PMs changes with the rotor position. Hence, the existing LPMC models are not suitable for HPM machine.

The novelty of this paper is to develop a LPMC model for HPM machine. Firstly, the model of PMs is divided and investigated to obtain the equivalent MMF of the HPM machine. Then, the branches of the LMPC are divided and established for the HPM machine based on a generalized approach [18]. In fact, this generalized approach was proposed to build the LPMC model for design of SPM machine, and the PM construction of HPM machine is similar to that of the SPM machine. The PM and air-gap are equivalent to the branches. Based on the developed branches, a nonlinear adaptive LPMC model

Received 22 January 2015, Accepted 6 March 2015, Scheduled 23 March 2015
* Corresponding author: Wenxiang Zhao (zwx@ujs.edu.cn).
The authors are with the School of Electrical and Information Engineering, Jiangsu University, Zhenjiang 212013, China.

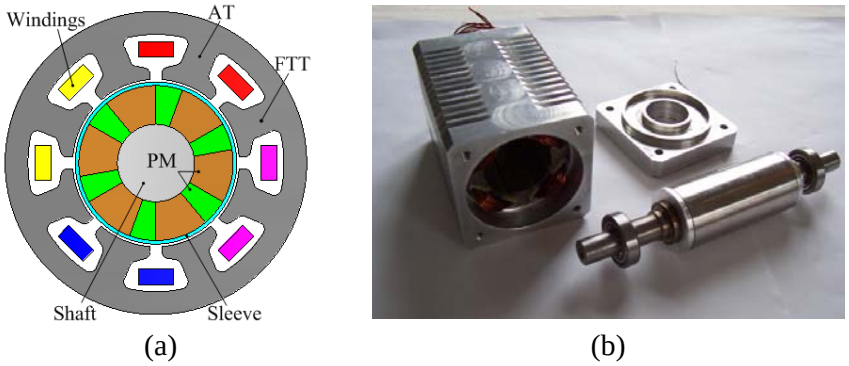

Figure 1. HPM machine. (a) Cross-sections. (b) Prototype machine.

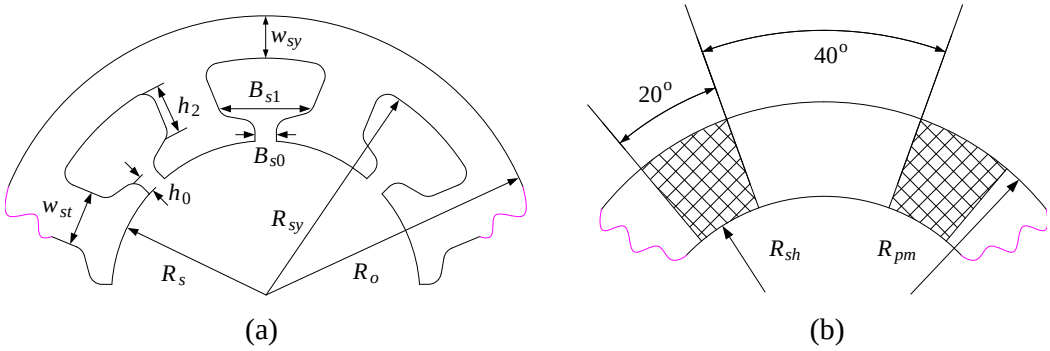

Figure 2. Detail parameters. (a) Stator. (b) Rotor.

for HPM machine is built to predict the electromagnetic performances, such as flux linkage, back-EMF, and torque.

In Section 2, the parameters of HPM machine will be presented. Then, the methods to divide PMs, establish the PMs model, obtain equivalent sinusoidal MMF of every branch and nonlinear adaptive LPMC model of HPM machine will be presented in Section 3. The HPM machine will be analyzed by using finite element method (FEM) and the proposed LPMC model, and the results will be compared and verified by the experiment in Section 4. Finally, some conclusions will be drawn in Section 5.

2. TEST MACHINE

Figure 1(a) shows the cross-section of the HPM machine. It can be seen that there are four armature teeth (AT) and four fault-tolerant teeth (FTT) in the stator. The single-layer concentrated winding is introduced into this machine to reduce copper loss. The single-layer concentrated winding has shorter end length than distributed field winding, hence saving copper winding. So, its copper loss decreases in the same current situation. Stainless steel sleeve is adopted to strengthen mechanical robustness of HPM. The 6-pole/8-slot 15 kW HPM machine is built as shown in Figure 1(b). Figure 2 shows the detailed parameters of the rotor and stator. The design dimensions and materials are listed in Table 1.

3. LUMPED PARAMETER MAGNETIC CIRCUIT MODEL

In fact, the LPMC has been a common technique for the analysis and design of electric machines by linking the material characteristics to the machine behavior. The magnetic field characteristics can be technically obtained using electric circuit principles, e.g., Kirchhoff's voltage law and Kirchhoff's current law. The basic principle of LPMC model can be expressed as

$$\Phi = FG \tag{1}$$

Table 1. Design specifications.

Items	Halbach machine
Rated power	15 kW
Number of PM poles (p)	6
Number of stator slot (N_s)	8
Based speed n_b (rpm)	14000
Stack length, l_s (mm)	73
Outside stator radius, R_o (mm)	43
Inside stator yoke radius, R_{sy} (mm)	36.5
Inside stator radius, R_s (mm)	23.75
Outside PM radius, R_{pm} (mm)	22
Inside shaft radius, R_{sh} (mm)	11
Slot opening height h_0 (mm)	3.0
Slot wedge height h_1 (mm)	1.0
Slot body height h_2 (mm)	8.87
Slot opening width Bs_0 (mm)	3.3
Slot wedge width Bs_1 (mm)	13.6
Width of teeth w_{st} (mm)	8.6
Air gap length h_g (mm)	0.75
Stator yoke width, w_{sy} (mm)	6.5
Coil turns per slot, N	45
PM type	SmCo24
B_r, (T)	1.01
H_c, (A/m)	−756000

where Φ, F and G are flux, MMF, and permeance of an element in the magnetic circuit, respectively. The permeance of a rectangular element can be given as

$$G = \mu_r \mu_0 \frac{S}{L} \tag{2}$$

where μ_r and μ_0 are the relative permeability and the permeability of air, respectively, and L and S are the effective length and cross-sectional area of the element, respectively.

The permeance of the PM, the air-gap, the stator and the yoke of stator can be given as

$$\begin{cases} S_{pm} = w_{pm} l_{pm} \\ G_m = \mu_r \mu_0 \frac{S_{pm}}{h_{pm}} \end{cases} \tag{3}$$

$$\begin{cases} S_g = l_s \left(R_s - \frac{h_g}{2} \right) \alpha_0 \\ G_{(0\ldots7)g} = \mu_0 \frac{S_g}{h_g} \end{cases} \tag{4}$$

$$\begin{cases} h_{sb} = h_0 \\ h_{st} = h_2 \\ h_{sy} = \left(\frac{R_o + R_{sy}}{2} \right) \theta_s \\ S_{sb} = l_s R_s \alpha_0 \\ S_{st} = l_s w_{st} \\ S_{sy} = l_s w_{sy} \\ G_{(0\ldots7)sb} = \mu_r \mu_0 \frac{S_{sb}}{h_{sb}} \\ G_{(0\ldots7)st} = \mu_r \mu_0 \frac{S_{st}}{h_{st}} \\ G_{(0\ldots7)sy} = \mu_r \mu_0 \frac{S_{sy}}{h_{sy}} \end{cases} \tag{5}$$

where h_{pm}, w_{pm} and l_{pm} are the magnet thickness, width and height, respectively. The μ_{pm} is the relative permeability of the PM. h_g, h_{sb}, h_{st} and h_{sy} are effective height of the air-gap, stator boot, stator teeth and stator yoke, respectively. S_g, S_{sb}, S_{st} and S_{sy} are effective cross-sectional area of the air-gap, stator boot, stator teeth and stator yoke, respectively. $G_{(0...7)sb}$ and $G_{(0...7)st}$ are the permeance of teeth-boot and teeth, respectively. α_0 and θ_s are the arc of boot at teeth and slot pitch, their values are 40° and 45°, respectively. l_s is stack length.

Since the variation of each phase magnetic circuit is identical, only one phase of the machine needs to be modeled. Here, phase-A is chosen as example, and its MMF can be obtained as

$$F_a = Ni_a \tag{6}$$

where N is the coil turns per stator slot, and i_a is the injected current of phase A.

3.1. PMs Model

The field distribution of HPM machine by FEM is shown in Figure 3. The arrows in each block indicate the magnetization directions of PMs. It can be observed that the right half of PM0, the left half of PM2 and PM1 form one magnetic flux loop. Then, the PM0 can be divided into left and right parts. Since the magnetization direction of PM0 is parallel, each part of PM0 can be also divided into two segments, marked as segment A and segment B (shown in Figure 4). As shown in Figure 4(a), the direction and value of the MMF are invariable in segment A because of the unchanged width of the PM. The direction of the MMF is invariable in segment B, but the value of the MMF is decreasing with the position because of the changed width of the PM. The value of MMF of segment B is zero at E and F points, while the value of the MMF of PM1 increases outward along the tangential direction, and the direction of PM1 is constant, as shown in Figure 4(b).

Magnetization (M) of PMs was resolved into radial and tangential components using the analytical model in [23–25]. Especially, a general analytical model of magnetization (M) was proposed to predict

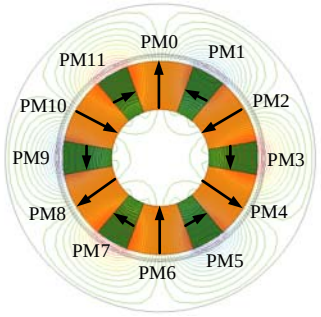

Figure 3. Field distribution.

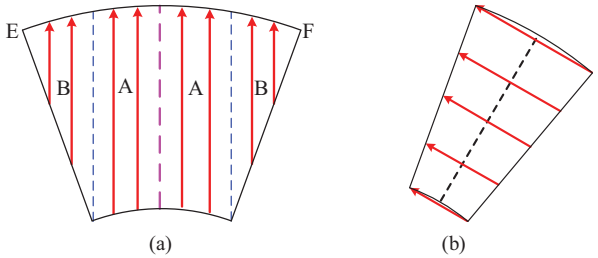

Figure 4. Direction and value of PMs. (a) PM0. (b) PM1.

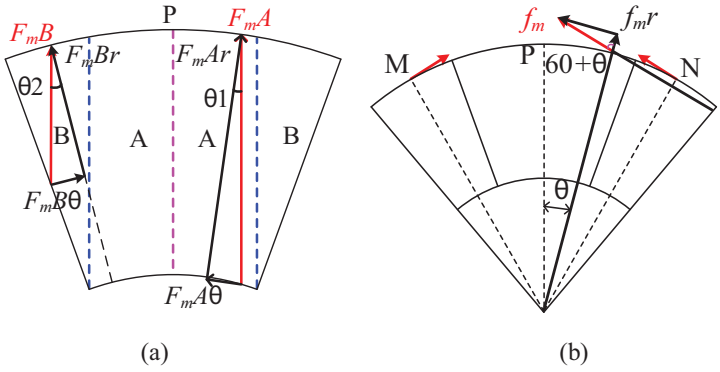

Figure 5. MMF resultant vector of PMs. (a) PM0. (b) PM1.

electromagnetic performance of PM brushless machines having segmented halbach array in [26]. Hence, in the LPMC model, the MMF of PMs should be resolved into the radial and tangential components. The MMFs of PM0 and PM1 are shown in Figure 5. Due to magnetic line of force is disjoint, point P is the critical separation point for adjacent magnetic circuit. There is only tangential component for M and N points, as shown in Figure 5(b). The direction of the radial component between M and N points is outward, which can be termed as one positive pole, and else are negative poles. The MMF, the radial and tangential components in segment A, segment B and PM1 can be obtained as

$$\begin{cases} \overrightarrow{F_mA} = \overrightarrow{F_mAr} + \overrightarrow{F_mA\theta} \\ F_mAr = F_mA * \cos\theta_1 \\ F_mA\theta = F_mA * \sin\theta_1 \\ \overrightarrow{F_mB} = \overrightarrow{F_mBr} + \overrightarrow{F_mB\theta} \\ F_mBr = F_mB * \cos\theta_2 \\ F_mB\theta = F_mB * \sin\theta_2 \\ \overrightarrow{f_m} = \overrightarrow{f_mr} + \overrightarrow{f_m\theta} \\ f_mr = f_m * \cos(\theta + 60) \\ f_m\theta = f_m * \sin(\theta + 60) \\ \overrightarrow{F_mr} = \overrightarrow{F_mAr} + \overrightarrow{F_mBr} + \overrightarrow{fmr} \\ \overrightarrow{F_m\theta} = \overrightarrow{F_mA\theta} + \overrightarrow{F_mB\theta} + \overrightarrow{f_m\theta} \end{cases} \tag{7}$$

where F_mA, F_mB and f_m are the MMF of segment A, segment B and PM1, respectively. F_mAr and $F_mA\theta$ are the radial and tangential components of F_mA, respectively. F_mBr and $F_mB\theta$ are the radial and tangential components of F_mB, respectively. f_mr and $f_m\theta$ are the radial and tangential components of f_m, respectively. θ, θ_1 and θ_2 are different mechanical angle at different position, respectively. F_mr and $F_m\theta$ are the MMF of the radial and tangential components of HPM, respectively.

3.2. LPMC Model

Figure 6 shows the open-circuit magnetic field distribution of test machine at 0° and 90° positions. The corresponding simplified actual magnetic circuits are shown in Figure 7. It can be known that each stator tooth is connected with segments A, B and one of assistant PM (i.e., PM1). Thus, the MMF of all PMs linked with one tooth can be equivalent to one effective MMF. G_y, G_{fm}, G_t and G_{Fm} are the permeance of the yoke, PM1, the tooth and half of PM0, respectively.

In this section, the branches of the LPMC are divided from stator teeth, and the PM and the air-gap are equivalent to every stator branch. Then, the value of the MMF varies at different positions. PM0 and PM1 are separated into 40 and 30 parts. As a result, one mechanical angle indicates one position. In this way, when the machine operates one electrical degree, the waveform of the equivalent MMF of PM (F_m curve) can be gained by (7), and shown in Figure 8. In order to verify its sinusoidal shape, an ideal sinusoidal fitting F_m curve is imported and compared with the predicted F_m curve. It

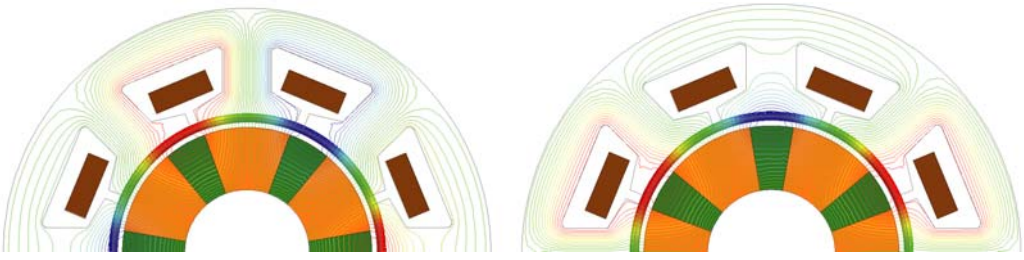

(a) (b)

Figure 6. Open-circuit magnetic field distribution. (a) Position = 0°. (b) Position = 90°.

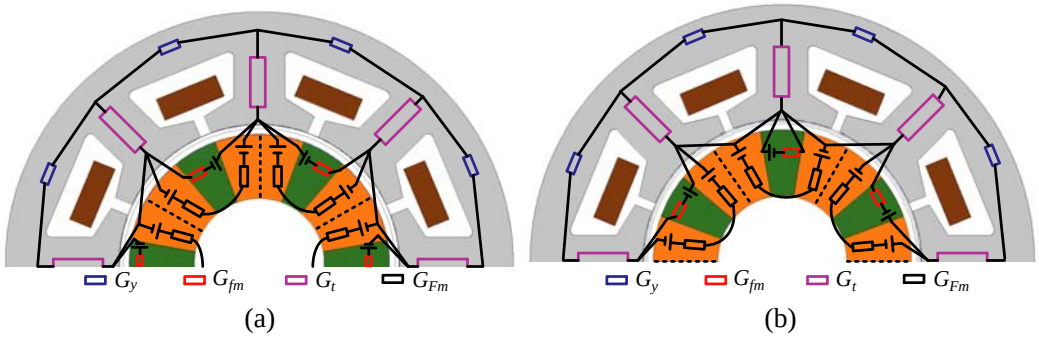

Figure 7. Simplified actual magnetic circuit. (a) Position = 0°. (b) Position = 90°.

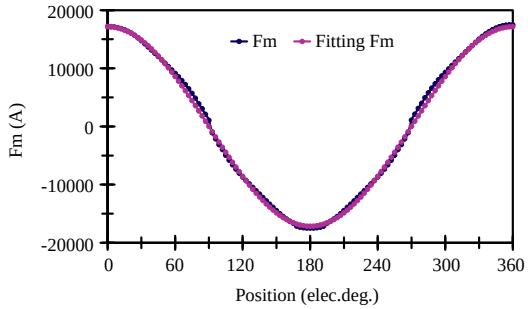

Figure 8. Equivalent MMF of PM in one electrical degree period.

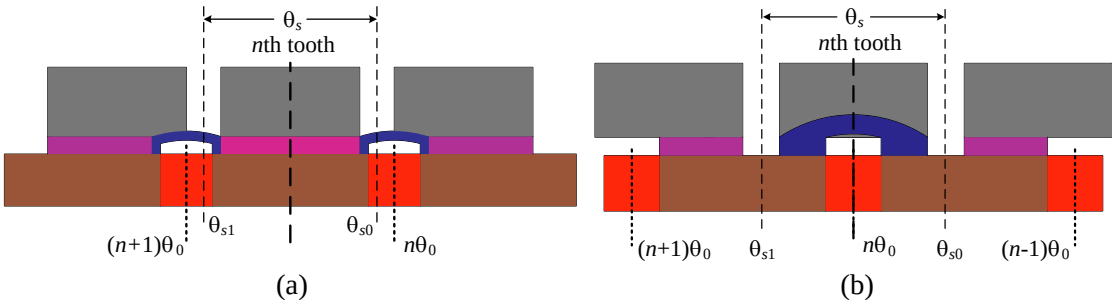

Figure 9. Equivalent MMF in a slot pitch. (a) One pole. (b) Two adjacent opposite poles.

can be concluded that there is only small discrepancy between the actual F_m and fitting F_m curve, and that this discrepancy is reasonable and expected because of partition and simplification of PMs. So, the equivalent MMF of PM can be given as

$$F_m(\theta) = F_m * \cos(p\theta) \tag{8}$$

where $F_m(\theta)$ is the value of the MMF under different electrical degree θ. p is number of pole-pairs. F_m is the maximum value of MMF.

Although the equivalent MMF of the stator teeth is changed by the relative position when the HPM machine is under operation, the relative positions of the PM and stator can be classified as two types. Figure 9 shows the relative position of the PM and the stator. First, a slot pitch is within one positive or negative pole, the flux produced by the PM flow throw the stator windings entirely, as shown in Figure 9(a). The equivalent MMF in a slot pitch can be obtained as

$$MMF = \int_{\theta_{s0}}^{\theta_{s1}} \frac{F_m(\theta)}{\theta_{s1} - \theta_{s0}} d\theta \tag{9}$$

where θ_{s0} and θ_{s1} are angles of both ends of nth tooth, respectively. $F_m(\theta)$ is the value of the MMF under different electrical degree θ.

Second, portion of two adjacent opposite pole are within a slot pitch, the contribution of flux from the magnet is mitigated due to the gap between the two adjacent opposite pole, as shown in Figure 9(b). The equivalent MMF in a slot pitch can be obtained as

$$MMF = \int_{n\theta_0}^{\theta_{s1}} \frac{F_m(\theta)}{\theta_{s1} - n\theta_0} d\theta - \int_{\theta_{s0}}^{n\theta_0} \frac{F_m(\theta)}{n\theta_0 - \theta_{s0}} d\theta \tag{10}$$

where $n\theta_0$ is the center angle of nth tooth.

The equivalent LPMC model of HPM machine is shown in Figure 10. It can be concluded that it is constituted by 8 branches according to stator teeth. In this model, the $\mathrm{PM}_{(0...7)}$ are the models of equivalent PM under a slot pitch. $G_{g(0...7)}$ are the models of the air gap. $\mathrm{AT}_{(0...4)}$ and $\mathrm{FT}_{(0...4)}$ are the models of AT and FTT, respectively. Also, it can be known that there are four layers in the LPMC model, and they stand for the layers of PM, the air, the stator and the yoke of stator along the radial direction from inside to outside, respectively. The adjacent layer connects with each other by permeance.

3.3. Final Solution

It can be known from Figure 10 that the node number of the equivalent LPMC model is 33. Meanwhile, the total node number keeps invariable with the position. For a magnetic circuit with N nodes, if some one node is chosen to be as reference node, the other $(N-1)$ nodes can be treated as independent. The MMF of reference node is zero, MMF difference between independent node and reference node are called node MMF, and thus, 32 independent nodes correspond to 32 nodes MMF. Meanwhile, 32^2 permeances exist in the LPMC model corresponding to 32 independent nodes, forming a permeance matrix $G(i,j)$, $(i,j = 0,1,2,\ldots,31)$. When $i = j$, permeance $G(i,j)$ is called self-permeance, otherwise, permeance $G(i,j)$ is called mutual-permeance. According to the foregoing developed LPMC model, the

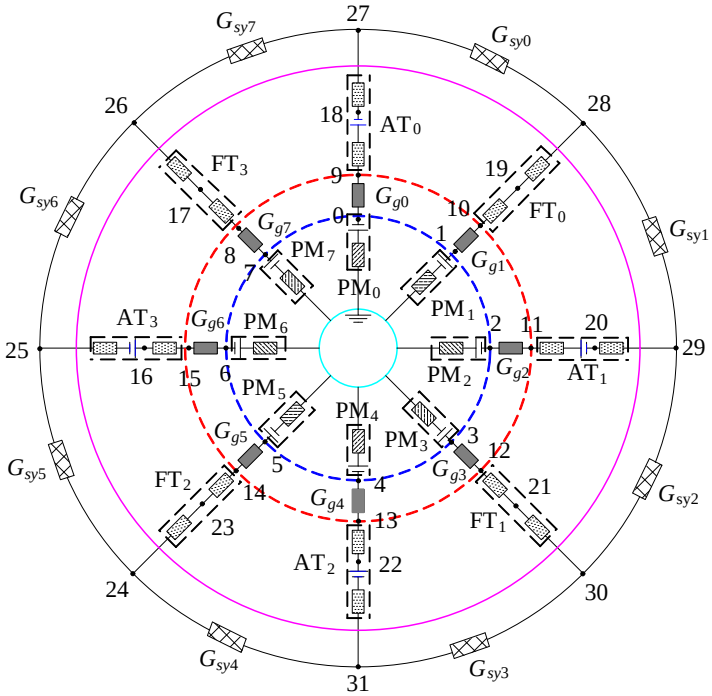

Figure 10. Proposed lumped parameter magnetic circuit model.

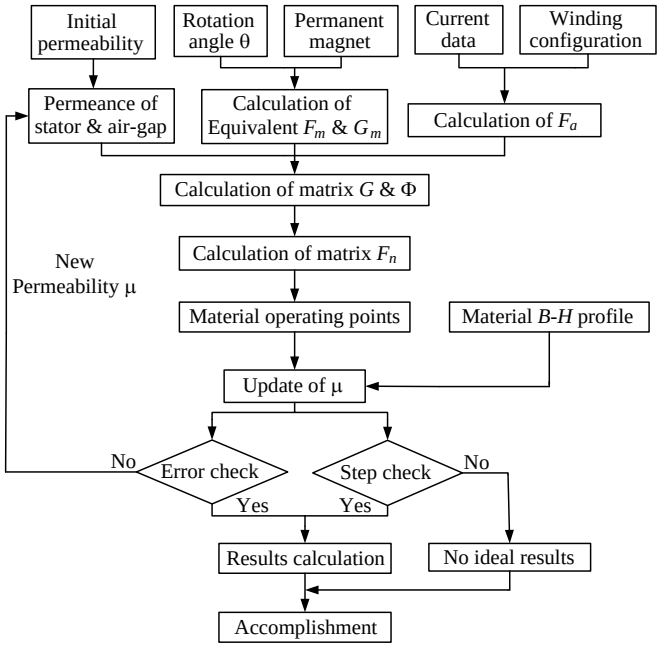

Figure 11. Iterative process of LPMC model.

node potential equation can be obtained by using (11).

$$\begin{bmatrix} G(0,0) & G(0,1) & \dots & G(0,31) \\ G(1,0) & G(1,1) & \dots & G(1,31) \\ \vdots & \vdots & \ddots & \vdots \\ G(31,0) & G(31,1) & \dots & G(31,31) \end{bmatrix} \begin{bmatrix} F_n(0) \\ F_n(1) \\ \vdots \\ F_n(31) \end{bmatrix} = \begin{bmatrix} \Phi_n(0) \\ \Phi_n(1) \\ \vdots \\ \Phi_n(31) \end{bmatrix} \tag{11}$$

viz. as

$$GF_n = \Phi \tag{12}$$

where G ($(0 \dots 31)$, $(0 \dots 31)$) is the permeance of node number, F_n $(0 \dots 31)$ the MMF of the node number, and Φ_n $(0 \dots 31)$ the flux of the node number. G, F_n and Φ are the matrix of permeance, MMF and the flux, respectively.

The iterative process of the LPMC model is shown in Figure 11. Firstly, the permeances of the stator and air-gap are calculated by using (4) and (5) based on the initial permeability. Secondly, the equivalent MMF (F_m) and permeance of PM (G_m) of every branch are obtained by rotation angle θ and PMs. Meanwhile, the MMF of each phase can be obtained by the current and winding configuration by using (6) when the HPM machine is under load. After all permeances in the LPMC model are prepared, the node potential equation can be built as (11).

Since nonlinear material WGT-200 is adopted in the stator core, a consecutive B-H table of the nonlinear material is listed to consider saturation effect. The Gauss-Seidel iterative method is adopted to improve the iterative speed. A new flux $\Phi_i^{(k)}$ and new flux density $B_i^{(k)}$ of the stator (i.e., AT_0) can be derived by using (13) and (14) after the initial permeability of the stator is applied to solve (11). A new magnetic intensity $H_i^{(k)}$ can be gained by considering where $B_i^{(k)}$ is located. Since the measured points are limited, when the value of $B_i^{(k)}$ is equal to the point of the table, $H_i^{(k)}$ is replaced by the value of the point. Else, when $B_i^{(k)}$ is located between two sampling points (N and $N+1$) of the nonlinear B-H table, the curve between two points is treated as a straight line, then, the $H_i^{(k)}$ can be written as (15). The corresponding relative permeability $\mu_i^{(k)}$ can be obtained as (16).

$$\Phi_i^{(k)} = \Phi_{t0}^{(k)} = G_{st0}\left(F_{18}^{(k)} - F_{27}^{(k)} - F_a^{(k)}\right) \tag{13}$$

$$B_i^{(k)} = \frac{\Phi_i^{(k)}}{S_{st}} \tag{14}$$

$$H_i^{(k)} = H_n + (H_{n+1} - H_n) \cdot \frac{B_i^{(k)} - B_n}{B_{n+1} - B_n} \tag{15}$$

$$\mu_i^{(k)} = \frac{B_i^{(k)}}{H_i^{(k)}} \tag{16}$$

$$\max\left(\left|\frac{B_i^{(k)} - B_i^{(k-1)}}{B_i^{(k)}}\right|\right) \leq \varepsilon \tag{17}$$

where ε is the set error precision.

Finally, the $\mu_i^{(k)}$ is fed back to the LPMC model to replace the initial permeability of the stator, thus one circulation of the iteration is achieved. If the values of kth and $(k-1)$th iteration flux densities ($B_i^{(k)}$ and $B_i^{(k-1)}$) are satisfied by (17), the iterative process is over. Otherwise, it will start next circulation before the iterations k is over the set calculation step, which is applied to prevent the process dropping into the endless loop.

4. SIMULATION AND EXPERIMENT VERIFICATIONS

To verify the accuracy of the proposed LPMC model for HPM machine, the time-stepping FEM and the experiment are employed to analyze the electromagnetic performances, such as flux density of the AT, the phase back-EMF, and the output torque.

The flux density of the armature tooth can be calculated by using proposed LPMC model, as shown in Figure 12(a). The FEM-based one is shown in Figure 12(b). It can be concluded that there is a good agreement between the FEM and the LPMC results.

Based on the solution of (13) and (14), and the back-EMF can be given as

$$e_a = -\frac{d\Psi_a}{dt} = -N\frac{d\Phi}{dt} = -NS_t\frac{dB}{dt} \tag{18}$$

where S_t is the effective cross-sectional area of the AT and Ψ_a the flux of the phase A.

Figure 13 compares the LPMC-based and FEM-based back-EMFs of the HPM machine at the rated speed of 14000 rpm with the measured one. It can be concluded that there is a good agreement in the shape and amplitude. Furthermore, the harmonic analyses of the back-EMF by using the LPMC model, the FEM and the experiment are shown in Figure 14, in which their THD are 0.52%, 4.6% and 1.6%, respectively. It can be known that the major harmonic order is 3th in the FEM result and 9th in the measured result. Although there is major discrepancy in third harmonic of the THD among the LPMC model, the FEM and the measured, it is acceptable by considering the saved-time because there

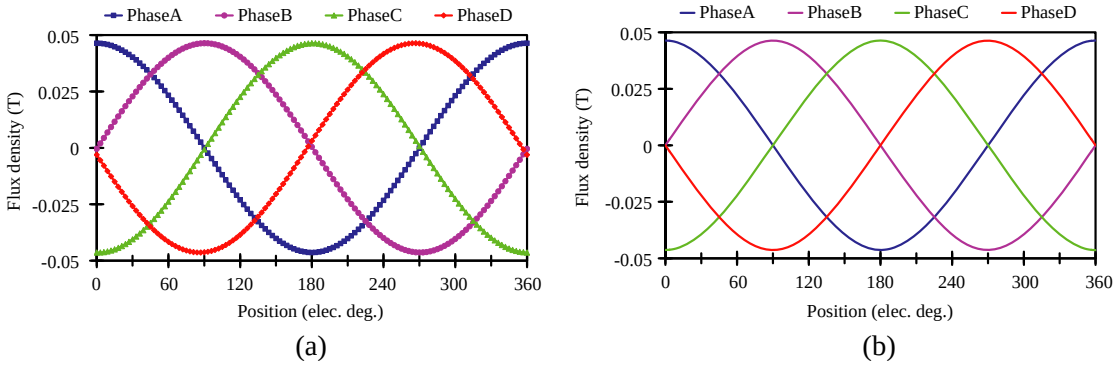

Figure 12. Flux density of AT_0. (a) LPMC model. (b) FEM.

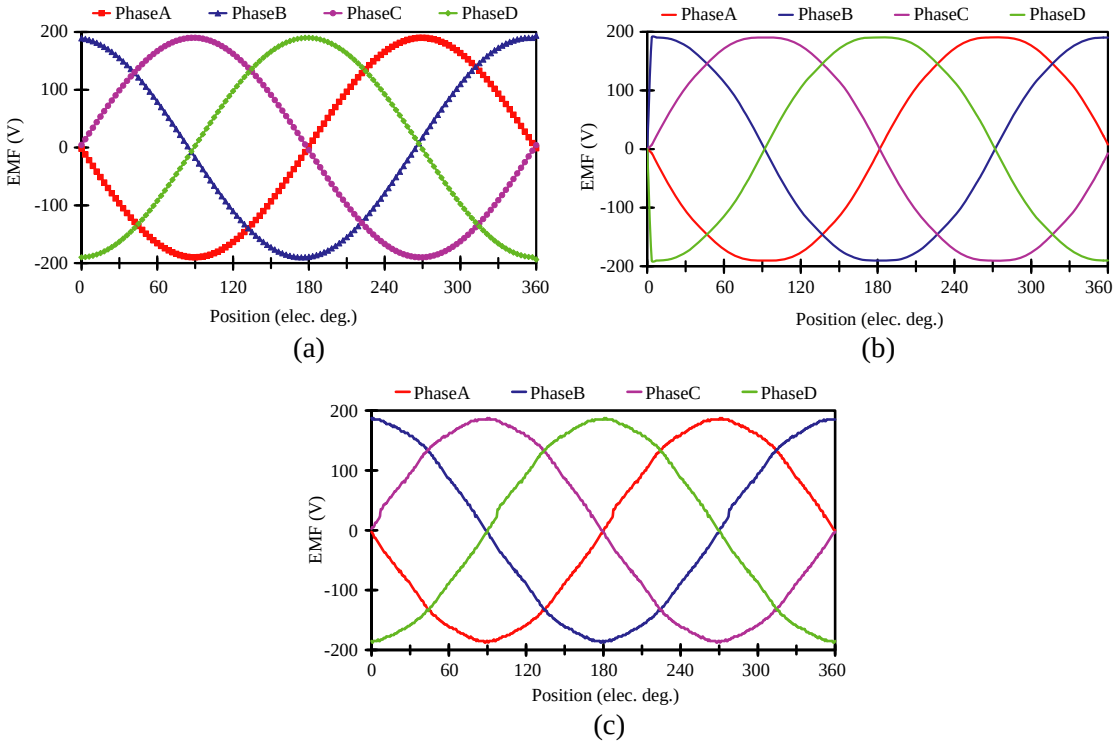

Figure 13. Back-EMF. (a) LPMC model. (b) FEM. (c) Measured.

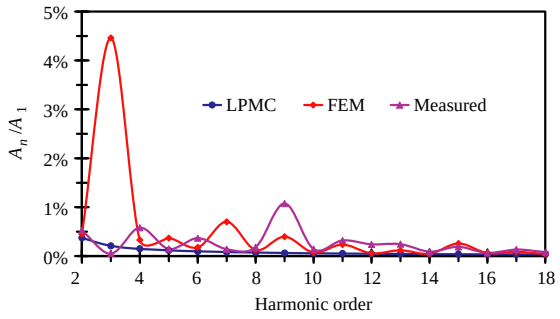

Figure 14. Harmonic analysis of back-EMF.

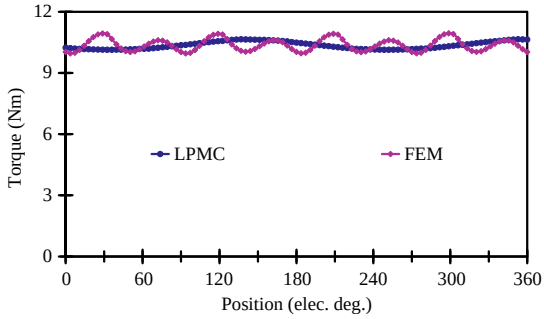

Figure 15. Torque.

are some predigestions in the LPMC model, and some errors exist in manufacture and installation of HPM machine and the effects of vibration and noise in the experiment.

The phase flux linkage and back-EMF of the machines can easily be obtained from the LPMC model. The electromagnetic torque can be predicted in terms of back-EMF and the current of each phase.

$$T_e = \frac{\sum\limits_{i=a\ldots d} e_i i_i}{w} \tag{19}$$

Figure 15 shows the predicted output torque when the sinusoidal phase current with 40 RMS is injected. Although the ripples of these results are different, the average torque of these results is almost same. The average value of the torque by FEM is 10.35 Nm, and the LPMC one is 10.37 Nm. It can be concluded that the proposed LPMC model is effective.

5. CONCLUSIONS

In this paper, a new method is proposed to divide and establish equivalent MMF for HPM machine, and the LPMC model of HPM machine is built based on equivalent MMF. The electromagnetic performances, e.g., the flux linkage, back-EMF, and torque performance, are obtained by the proposed LPMC model. From the comparison of the results among the LPMC model, the FEM and the experiment, the effectiveness of proposed LPMC model is verified.

ACKNOWLEDGMENT

This work was supported by the National Natural Science Foundation of China (Projects 61273154, 51422702 and 51477068), by the Specialized Research Fund for the Doctoral Program of Higher Education of China (Project 20123227110012), by the Natural Science Foundation of Jiangsu Province (Project BK20130011), and by the Priority Academic Program Development of Jiangsu Higher Education Institutions.

REFERENCES

1. Zhu, Z. Q. and D. Howe, "Halbach permanent magnet machines and applications: A review," *IEE Proc. Electr. Power Appl.*, Vol. 148, No. 7, 299–308, Jul. 2011.
2. Popa, D.-C., V.-I. Gliga, and L. Szabó, "Theoretical and experimental study of a modular tubular transverse flux reluctance machine," *Progress In Electromagnetics Research*, Vol. 139, 41–55, 2013.
3. Ding, W., Z. Yin, L. Liu, J. Lou, Y. Hu, and Y. liu, "Magnetic circuit model and finite-element analysis of a modular switched reluctance machine with E-core stators and multi-layer common rotors," *IET Electr. Power Appl.*, Vol. 8, No. 8, 296–309, 2014.
4. Aravind Vaithilingam, C., N. Misron, I. Aris, M. H. Marhaban, and M. Nirei, "Electromagnetic design and FEM analysis of a novel dual-air-gap reluctance machine," *Progress In Electromagnetics Research*, Vol. 140, 523–544, 2013.
5. Lin, D., P. Zhou, S. Stanton, and Z. J. Cendes, "An analytical circuit model of switched reluctance motors," *IEEE Trans. on Magn.*, Vol. 45, No. 12, 5368–5375, Dec. 2009.
6. Kokernak, J. M. and D. A. Torrey, "Magnetic circuit model for the mutually coupled switched-reluctance machine," *IEEE Trans. on Magn.*, Vol. 36, No. 2, 500–507, Mar. 2000.
7. Xu, Z., S. Xie, and P. Mao, "Analytical design of flux-switching hybrid excitation machine by a nonlinear magnetic circuit method," *IEEE Trans. on Magn.*, Vol. 49, No. 6, 3002–3008, Jun. 2013.
8. Zhu, Z. Q., Y. Pang, D. Howe, S. Iwasaki, R. Deodhar, and A. Pride, "Analysis of electromagnetic performance of flux-switching permanent-magnet machines by nonlinear adaptive lumped parameter magnetic circuit model," *IEEE Trans. on Magn.*, Vol. 41, No. 11, 4277–4287, Nov. 2005.
9. Zhou, S., H. Yu, M. Hu, C. Jiang, and L. Huang, "Nonlinear equivalent magnetic circuit analysis for linear flux-switching permanent magnet machines," *IEEE Trans. on Magn.*, Vol. 48, No. 2, 883–886, Feb. 2012.
10. Cheng, M., K. T. Chau, C. C. Chan, E. Zhou, and X. Huang, "Nonlinear varying-network magnetic circuit analysis for doubly salient permanent-magnet motors," *IEEE Trans. on Magn.*, Vol. 36, No. 1, Part 2, 339–348, 2000.
11. Kano, Y., T. Kosaka, and N. Matsui, "A simple nonlinear magnetic analysis for axial-flux permanent-magnet machines," *IEEE Trans. on Ind. Electron.*, Vol. 57, No. 6, 2124–2133, Jun. 2010.
12. Tarmer, İ., "Designing an efficient permanent magnet generator for outdoor utilities," *Int. J. Eng. Science Inno. Tech.*, Vol. 3, No. 3, 543–548, 2014.
13. Chen, Q., G. Liu, W. Zhao, and M. Shao, "Nonlinear adaptive lumped parameter magnetic circuit analysis for spoke-type fault-tolerant permanent-magnet motors," *IEEE Trans. on Magn.*, Vol. 49, No. 9, 5150–5157, Sep. 2013.

14. Hemeida, A. and P. Sergeant, "Analytical modeling of surface PMSM using a combined solution of Maxwell's equations and magnetic equivalent circuit," *IEEE Trans. on Magn.*, Vol. 50, No. 12, 7027913, Dec. 2014.
15. Jung, M. S., S. J. In, K. J. Hyun, and S. R. Jong, "Analysis of overhang effect for a surface-mounted permanent magnet machine using a lumped magnetic circuit model," *IEEE Trans. on Magn.*, Vol. 50, No. 5, 1–7, 2014.
16. Kazan, E. and A. Onat, "Modeling of air core permanent-magnet linear motors with a simplified nonlinear magnetic analysis," *IEEE Trans. on Magn.*, Vol. 47, No. 6, 1753–1762, Jun. 2011.
17. Hsieh, M. F. and Y. C. Hsu, "A generalized magnetic circuit modeling approach for design of surface permanent-magnet machines," *IEEE Trans. on Ind. Electron.*, Vol. 59, No. 2, 779–792, Feb. 2012.
18. Kemmetmuller, W., D. Faustner, and A. Kugi, "Modeling of a permanent magnet synchronous machine with internal magnets using magnetic equivalent circuits," *IEEE Trans. on Magn.*, Vol. 50, No. 6, Part 2, 8101314, Jun. 2014.
19. Zhu, L., S. Z. Jiang, Z. Q. Zhu, and C. C. Chan, "Analytical modeling of open-circuit air-gap field distributions in multi-segment and multilayer interior permanent-magnet machines," *IEEE Trans. on Magn.*, Vol. 45, No. 8, 3121–3130, Aug. 2009.
20. Lovelace, E. C., T. M. Jahns, and J. H. Lang, "A saturating lumped-parameter model for an interior PM synchronous machine," *IEEE Trans. on Ind. Appl.*, Vol. 38, No. 3, 645–650, May–Jun. 2002.
21. Seo, J. H. and H. S. Choi, "Cogging torque calculation for IPM having single layer based on magnetic circuit model," *IEEE Trans. on Magn.*, Vol. 50, No. 10, 8102104, Oct. 2014.
22. Markovic, M. and Y. Perriard, "Optimization design of a segmented halbach permanent-magnet motor using an analytical model," *IEEE Trans. on Magn.*, Vol. 45, No. 7, 2955–2960, Jul. 2009.
23. Rahideh, A. and T. Korakianitis, "Analytical magnetic field distribution of slotless brushless machines with inset permanent magnets," *IEEE Trans. on Magn.*, Vol. 47, No. 6, Part 2, 1763–1774, Jun. 2011.
24. Yan, L., L. Zhang, T. Wang, Z. Jiao, C. Y. Chen, and I. M. Chen, "Magnetic field of tubular linear machines with dual Halbach array," *Progress In Electromagnetics Research*, Vol. 136, 283–299, 2013.
25. Shen, Y. and Z. Q. Zhu, "General analytical model for calculating electromagnetic performance of permanent magnet brushless machines having segmented Halbach array," *IET Electr. Syst. Transp.*, Vol. 3, No. 3, 57–66, 2013.